Arch. Metall. Mater. **64** (2019), 1, 285-292

DOI: 10.24425/amm.2019.126250

ZHONGWEI MA*, LIN MA*, BO XU**#, CHUCHEN DAN**,
ZHAOKUN HE**, YUE WANG*#

HIGH CYCLE FATIGUE PERFORMANCE OF HOLLOW-EXTRUDED 6005A-T6 ALUMINUM ALLOY CHARACTERIZED BY A LAYERED MICROSTRUCTURE

Sound joint of hollow-extruded 6005A-T6 aluminum alloy was achieved by friction stir welding and its high cycle fatigue performance was mainly investigated. As a result, the joint fatigue limit reaches 128.1 MPa which is 55% of the joint tensile strength. The fatigue fracture mainly occurs at the boundary between the stir zone and thermo-mechanically affected zone due to the large difference in the grain size. This difference is caused by the layered microstructure of the base material. The shell pattern with parallel arcs is the typical morphology in the fracture surface and the distance between arcs is increased with the increase of stress level. The specimen with the fracture located in the stir zone possesses a relatively low fatigue life.

Keywords: Friction stir welding, Hollow-extruded 6005A-T6 aluminum alloy, Fatigue, Fracture, Microstructure

1. Introduction

The increasing requirements of high strength and low weight strongly motivate the application of light alloys in the fields of automotive, aerospace and high-speed train [1-3]. Hollow-extruded aluminum alloy (HEAA) profile is widely used in the safety critical frame structures of automotive and high railway because it integrates the function of beams and plates and then can reduce the number of components and joints, thereby improving the reliability of metal structures. Since the HEAA profile inevitably undergoes the dynamical load in the service, its fatigue properties have received high attention. The fatigue properties of HEAA profile are predominated by several factors including microstructure, loading mode, joining method and so on. Nanninga et al. [4-6] have verified that the fatigue properties of HEAA profile were influenced by the surface finish, extrusion welds, extrusion die line and load direction. When it comes to the manufacture of large HEAA profile, weld is inevitable [7]. However, the welded joint is prone to be the potential weak position where the fatigue fracture occurs. In fact, fatigue is the principal cause of failure for welded joint, which has a significant influence on the reliability of the whole HEAA profile [8,9].

Friction stir welding (FSW), a solid-state joining technology, is widely applied in the welding of low-melting-point alloys [10-14]. It has been shown that the FSW joint possesses superior fatigue properties compared with the fusion welding joint, which is attributed to the avoided defects of porosity, severe deformation and hot crack resulting from the excessive heat input [9]. Although the fatigue properties of FSW joint were investigated by many researchers [15-17], there are limited literatures on the fatigue performance of FSW joint of HEAA profile. In fact, the plates of some HEAA profiles possess a layered microstructure comprised of fully recrystallized outer layers and a fibrous inner layer [18]. The FSW joint fatigue performance of this microstructure is still missing. 6005A-T6 alloy is a middle-strength aluminum alloy and possesses a good corrosion resistance [19]. This aluminum alloy is the main base material (BM) in the production of HEAA profile because of its excellent extrusion property. Since the HEAA profile FSW joint links with the supporting rib (Figs. 1a and b), the joint mechanical properties are not only influenced by the microstructure but also by the structural characteristic. Liu et al. [20] investigated the tensile properties of the HEAA profile FSW joints with and without the supporting rib. Results showed that the rib only made the fracture did not occur at the joint advancing side (AS) due to the relatively large load bearing area (Figs. 1a and b) and the joint retreating side (RS) without linking the supporting rib was the dominated part influencing the joint fracture. This study placed the emphasis on the relationship between the microstructure and fatigue properties. Therefore, the tensile fatigue properties of 6005A-T6 HEAA FSW joint without the supporting rib were investigated, and this HEAA profile possesses the above-mentioned layered microstructure. The high cycle fatigue tests were conducted and the microstructure, microhardness, fracture location and fracture surface of the joint were analyzed.

* SHENYANG AEROSPACE UNIVERSITY, SCHOOL OF AEROSPACE ENGINEERING, SHENYANG, CHINA
** CRRC SIFANG CO., LTD, QINGDAO 266111, CHINA
# Corresponding authors: Xubopaper2018@163.com, endlesswy@163.com

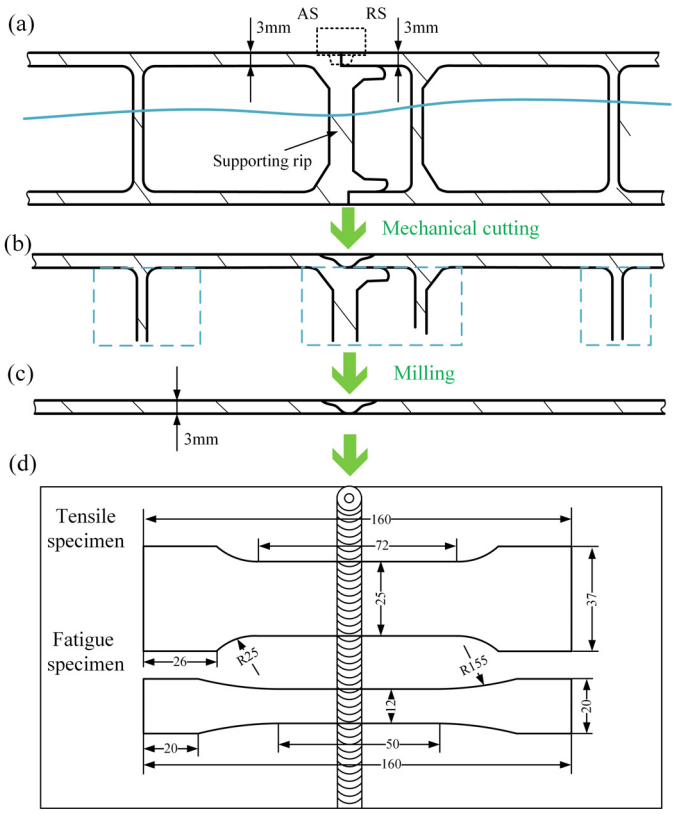

Fig. 1. (a)-(c) Preparation processes of joint; (d) schematics of tensile and fatigue specimens

2. Experimental procedure

The cross section of HEAA profile and the joint configuration are displayed in Fig. 1a. Based on the earlier stage of present study, one optimized process parameters combination was chosen, to obtain the high quality FSW joint. The parameters were selected as following: rotational speed of 1600 rpm, welding speed of 600 mm/min and plunge depth of 0.2 mm. The tool consisted of a six-groove shoulder with 10 mm diameter and a conical threaded pin with 2.8 mm length. Pin top and bottom diameters were 3 mm and 5 mm, respectively. After welding, there was an elapsed time of a week before the subsequent investigation. Firstly, cutting machine was used to separate the profile (Fig. 1a). Secondly, a milling machine was used to remove the ribs (Fig. 1b). Finally, the plate containing the 3 mm thick FSW joint was acquired (Fig. 1c). Vickers microhardness tests were performed at the top, middle and bottom of the joint cross section under a load of 200 g for a dwell time of 10 s, and the distance between two tested points was 0.5 mm. According to ISO 4136:2001 and ISO 12107:2003, the tensile and fatigue specimens were respectively fabricated, and their schematics are displayed in Fig. 1d. The tensile tests were performed under a speed of 3 mm/min at the room temperature. Prior to the fatigue tests, the specimen surface was ground and polished to remove any potential defects such as shoulder marks, lack of penetration and so on. The uniaxial tension fatigue tests at room temperature were carried out on a high-frequency fatigue test machine under a stress ratio of R (σ_{min} / σ_{max}) = 0.06 at the sinusoidal frequency of 10 Hz. Ten stress levels ranging from 53%~85% of the joint tensile strength were used to evaluate the fatigue limit during fatigue tests. The stress gap between two levels gradually reduced when the fatigue life of specimen was close to the aimed cycles (10^7). Fatigue probability and confidence coefficient were selected as 50% and 90%, so three samples were tested at each stress level according to ISO 12107:2003. Statistical analysis was used to acquire the *S-N* curve, by which the fatigue limit of the joint can be assessed. In this study, microstructure observations were performed to understand the fatigue fracture mechanism of FSW joint of HEAA profile with a layered microstructure. The metallurgical observation was performed on the cross section of the joint and BM by an optical microscope (OM, Olympus-GX71). Before the observation, samples were polished and then etched by Keller's reagent. The surface of fatigue fracture was examined by a scanning electron microscope (SEM, SU3500).

3. Results and discussion

3.1. Microstructure

Fig. 2a shows that the BM is characterized by a layered microstructure. The outer layers are comprised of coarse grains with the sizes ranging from 200 μm to 1000 μm, which is attributed to the recrystallization induced by the high stored strain energy accumulating in the surface of the base plate during the extrusion process. By contrast, the inner layer possesses a fibrous microstructure due to the extruded material flow (Fig. 2b). As shown in Fig. 2c, sound joint without void, and crack defects are obtained. The cross section can be divided into stir zone (SZ), thermo-mechanically affected zone (TMAZ), heat affected zone (HAZ) and BM. The thickness of coarsened outer layers is gradually decreased from BM to the SZ due to the tool stirring action, resulting in an opened morphology of inner layer. The inner layer and two outer layers with different microstructures eventually merge into a uniform microstructure in the SZ. The SZ presents a basin shape which is related to the tool geometry and the distribution of heat generation [21]. The onion ring is formed in the SZ due to the combined effect of welding heat and material flow [22]. The enlarged views of the SZ bottom and top are respectively displayed in Figs. 2e and f. The original grains of BM including the large recrystallization grains in outer layers and the elongated grains in inner layer are all transformed into fine-equiaxed grains due to the dynamic recrystallization induced by the intense plastic deformation and thermal cycle [23,24]. Moreover, the grains near the SZ top surface are finer than that near the SZ bottom surface (Figs. 2e and f), which results from the more intense stirring action induced by the tool shoulder at the SZ top. The refined grains improve the resistance of fatigue crack initiation and then contribute to increasing the initiation life of fatigue crack [25,26]. The grains in the TMAZ present a further elongated and bended morphology (Fig. 2d), resulting from the driving action by the high-flow-velocity materials in

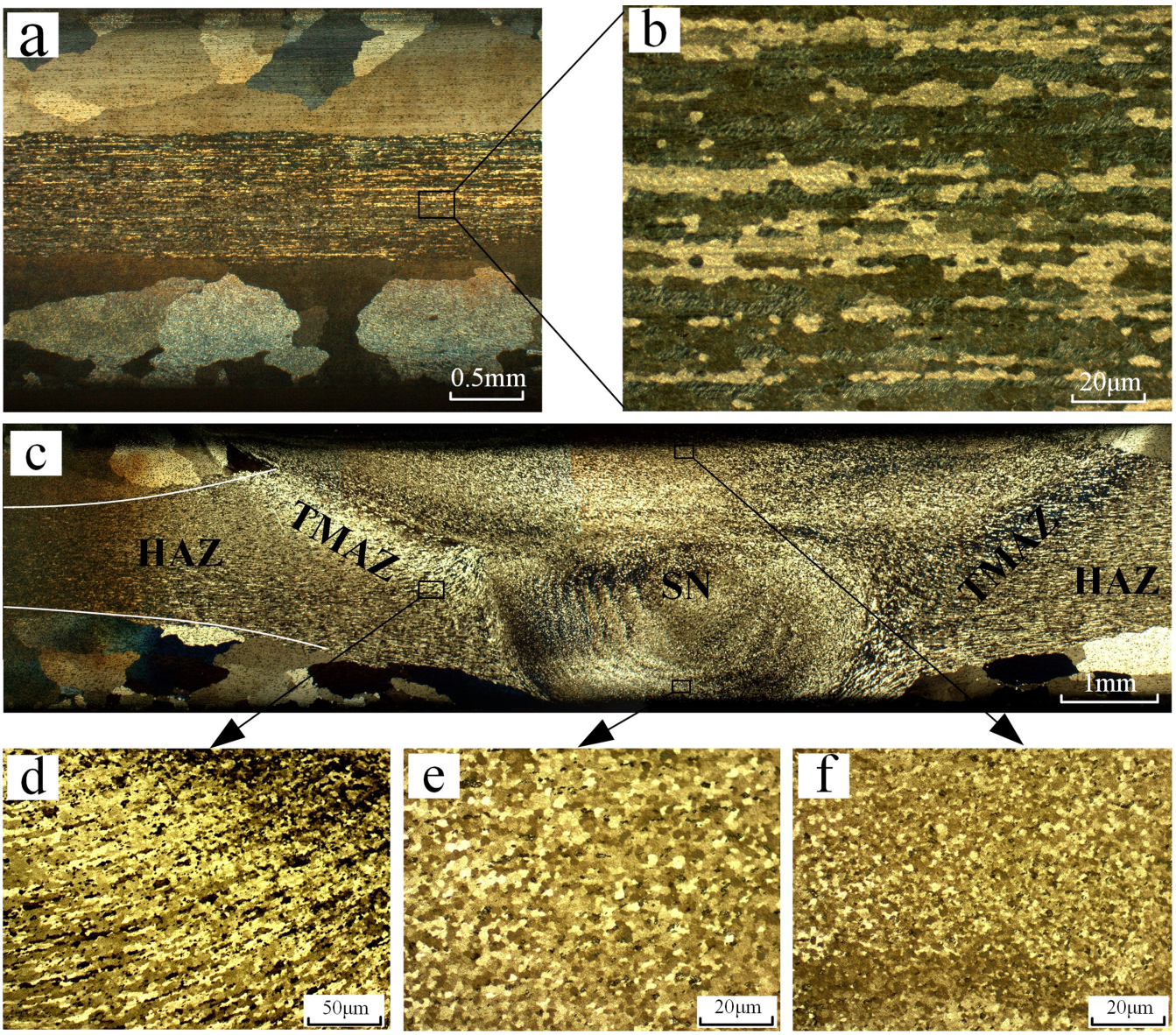

Fig. 2. Microstructure of cross sections: (a) BM, (b) enlarged view of BM, (c) FSW joint, (d) TMAZ, (e) SZ bottom and (f) SZ top

the SZ [27]. The boundary between the SZ and TMAZ at AS is clear than that at RS (Fig. 2c), which is related to the difference in force condition and thermal cycle [20,28,29].

3.2. Microhardness and tensile properties

Fig. 3 depicts the microhardness distributions at the top, middle and bottom of the cross section. The microhardness distributions of these tested regions present a similar changing trend from BM to SZ. The microhardness first quickly decreases from BM to HAZ and then slightly increases from TMAZ to SZ, which results in a 'W-shaped' profile. The microhardness of the joint is influenced by several factors mainly including precipitate phase, grain size and grain dislocation [7,20]. 6005A-T6 alloy is an age-hardening alloy, and its microhardness is sensitive to the transformation of precipitate phase [30]. The lowest-microhardness region is located at the HAZ of AS and is very close to the TMAZ, which is attributed to the precipitate transformation and grain coarsening induced by the thermal cycle during the FSW process. Although the transformation of precipitate also occurs in the SZ and TMAZ, the grains at these two zones play a positive role in increasing the microhardness. The severely deformed grains in the TMAZ contain higher dislocation density than those in HAZ, which results in a higher microhardness [20]. The relationship between grain size and microhardness can be described by Hall-Petch relationship, $HV = HV_0 + kd - 1/2$, where HV is the value of Vickers microhardness of the polycrystalline metal, HV_0 and k are constants, and d is the regional grain size [31]. This relationship illustrates that the decreased grain size is beneficial to increasing the microhardness. The grain size in the SZ is less than 10 μm which is far smaller than that in other zones. Therefore, the microhardness in the SZ is higher than that in the TMAZ or HAZ. For the same reason, the average microhardness valve of BM in inner layer (Middle in Fig. 3) is also higher than that in outer layers (Top and Bottom

TABLE 1

Results of fatigue tests

Group number	1	2	3	4	5	6	7	8	9	10
Stress level	85%	75%	70%	65%	62%	60%	58%	56%	54%	53%
S/MPa	200.6	177	165.2	153.4	146	141.6	136.9	132.2	127.5	125
N	31739	129279	455229	812364	1288219	2966497	6177436	8677446	10^7	10^7

in Fig. 3). The average microhardness values of tested region in the SZ from top to bottom are respectively 78 HV, 75 HV and 73 HV, which is mainly because the grain size at the SZ top is smaller than that at the SZ bottom. The softened region at the joint top is wider than that at the joint bottom, which coincides with the basin shape of the SZ. Fig. 4 displays the Engineering stress-strain curves of BM and FSW joint. The fracture location of FSW joint corresponds to the lowest-microhardness region. The ultimate tensile strength and elongation of FSW joint are 233 MPa and 5.7%, which are 81.7% and 54.2% of those of BM, respectively. These tensile properties are excellent for 6005A-T6 alloy FSW joint referring to the reported literatures [19,20,30].

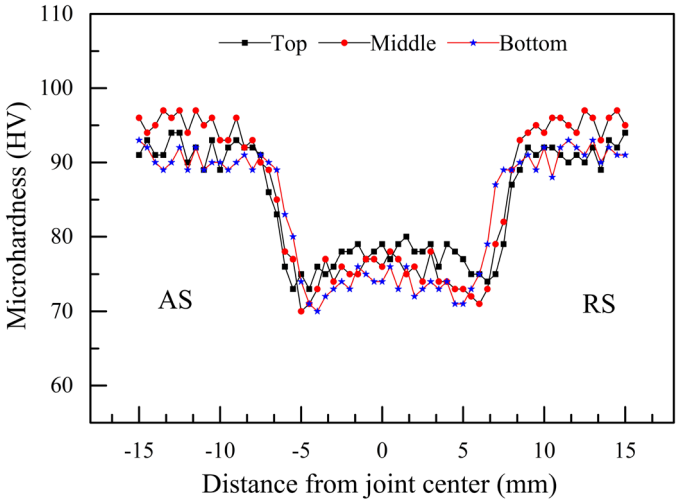

Fig. 3. Microhardness profiles

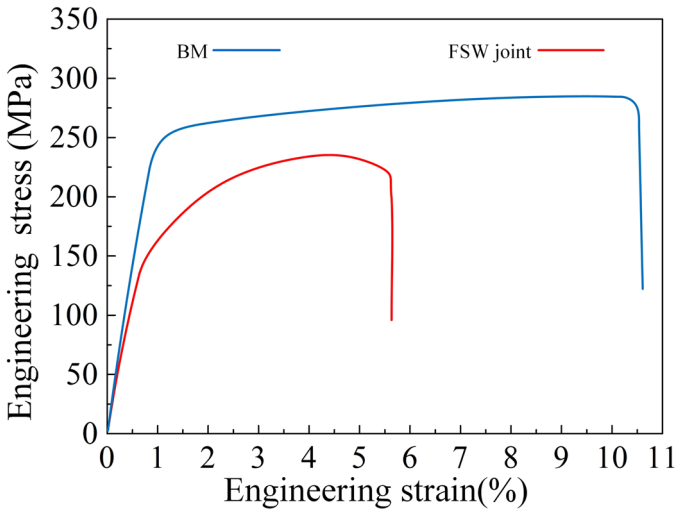

Fig. 4. Engineering stress-strain curves

3.3. Fatigue properties

Table 1 shows the fatigue data of FSW joints. *S* is the maximum stress (σ_{max}), and *N* is the media fatigue life calculated by the function of $N = \sqrt[n]{N_1 \cdot N_2 \ldots N_n}$. When the stress level varies from 85% to 53%, the value of fatigue life increases in the range of 10^5-10^7. Based on the data in Table 1, a rectangular coordinate system is established. The maximum stress and the corresponding fatigue life are respectively represented by the vertical and horizontal coordinates (Fig. 5). It is found that the fatigue life distribution under the higher stress level is more concentrated than that under lower stress level. This result demonstrates that with the decrease of stress level, the increase of joint fatigue life becomes more and more obvious. The relationship between the maximum stress and the fatigue life can be described by a *S*-*N* curve, and the following power function is generally used to obtain this curve.

$$S^m \cdot N = C \tag{1}$$

C and m are the constants which are related to the material, stress ratio and stress loading mode. In order to achieve an explicit relationship between the maximum stress and the fatigue life, Eq. 1 can also be expressed by the following form.

$$S = C^{\frac{1}{m}} \cdot N^{-\frac{1}{m}} \tag{2}$$

Based on least-squares fitting, the result of regression line is displayed as Eq. 3 and the fitting result is presented in Fig. 5.

$$S = 441.2305 N^{-0.07671} \tag{3}$$

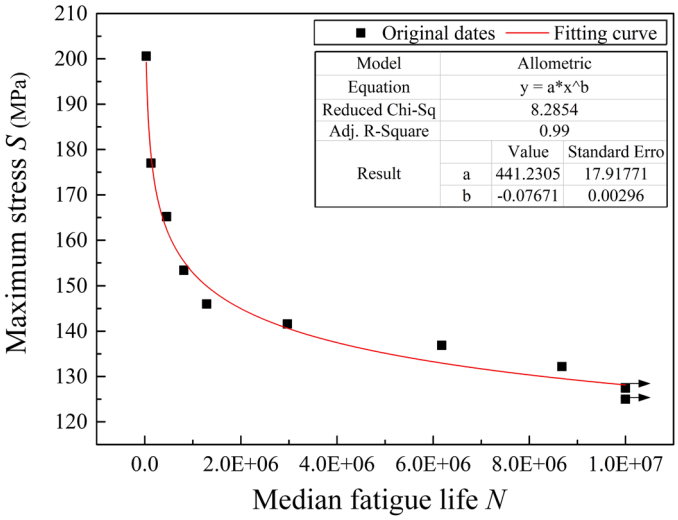

Fig. 5. S-N curve of FSW joint

The correlation coefficient of the fitting result is 0.99, illustrating that the acquired fitting function coincides well with the experiment results. In this study, the minimum σ_{max} is regarded as the fatigue limit, when the cycle number of the stress reaches 10^7. According to Eq. 3, the fatigue limit is 128.1 MPa which reaches 55% of the joint tensile strength. The fatigue limit of FSW joint is generally higher than that of TIG or MIG joint. Zhou et al. [32] reported that the fatigue limit of FSW joint was about 65% higher than that of MIG joint due to the sound structure, finer grain in the SZ and rather lower residual stress of FSW joint. Moreover, Ericsson et al. [33] found that the FSW joint possessed a higher fatigue life compared MIG and TIG joints and the scatter of its fatigue life was smaller due to the high repeatability of FSW process.

3.4. Fracture analysis

Fig. 6 presents the fracture locations of the fatigue specimens. Most of the specimens fracture at the boundary between SZ and TMAZ and there is no preference between AS and RS (Fig. 6a). This result is different from observations of Xu et al. [1], Aydin et al. [17] and He et al. [34]. According to their studies, the FSW joint is prone to fracture at the lowest-microhardness location under high-cycle fatigue test. This difference is the result of the large grains in the outer layers of BM used in this study, which is discussed in the following part in detail. A few specimens fracture in the SZ (Fig. 6b) and their fatigue life is relatively low compared with those fracturing at the boundary between SZ and TMAZ under the same stress level. More than 90% of the fatigue life of defect-free metal is spent on fatigue crack initiation and propagation. The crack initiation and propagation are extremely sensitive to the internal defects. The zigzag curve defect is formed in the SZ due to the remnant of oxide layer, which is detrimental to the joint fatigue properties [8].

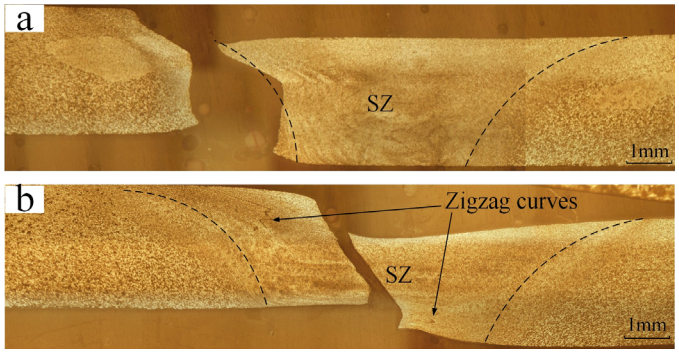

Fig. 6. Cross sections of specimen fracturing at (a) boundary between SZ and TMAZ, (b) SZ

Fig. 7 shows the fracture surface morphologies of the specimens under different stress levels. The fracture surface is comprised of three typical regions: crack initiation region, crack propagation region and final fast fracture region. As shown in Fig. 7a, a shell pattern is formed in the fracture surface of the specimen with the fatigue life of 7866321 cycles under the stress level of 56%. The shell pattern consists of the crack initiation and propagation regions, and the fatigue source is located in its root region. A coarse grain can be observed from the enlarged view in the crack initiation region (Fig. 7b), which is the unbroken large grain of the surface layer outside SZ. After the initiation, the fatigue crack extends to the joint inner region roughly along the boundary between SZ and TMAZ (Fig. 6a), resulting in the crack propagation region. Besides the second cracks, plastic fatigue striations, which is perpendicular to the extending direction of crack, are observed from the enlarged view of crack propagation region (Fig. 7c). Moreover, several parallel arcs are formed near the edge of the crack propagation region (Fig. 7a), and the gap between the arcs is ~0.13 mm at the position with 1.85 mm away from the crack source. The final fracture region presents a ductile fracture characterized by dimpled morphologies, and the rod-like second phases are located in some large dimples (Fig. 7d).

Fig. 7e shows the fracture surface of the specimen with the stress level of 62%. The fatigue crack initiates at the joint bottom surface where a large grain with a size of ~200 μm is located (Fig. 7f). Referring to the crack source in Figs. 7a and b, it is concluded that the existence of large grains outside the SZ at the joint bottom easily leads to the initiation of fatigue crack under high-cycle fatigue in this study. Due to the layered microstructure of BM, the influence of microstructural heterogeneity becomes more obvious, which is illustrated by the site of fatigue crack source in this study. Generally, the preferred initiation site of the fatigue crack is associate with the welding defect, inclusion, loading direction and so on. For the FSW joint without welding defect, the fatigue crack initiation site is mainly influenced by the microstructural heterogeneity. Deng et al. [9] found that for the FSW joint without welding defect, the fatigue failure mainly occurred in the TMAZ or HAZ, which was attributed to the large microstructural heterogeneity. Aydin et al. [17] reported that the inhomogeneous microstructure in the joint raised the stress concentration, which facilitated the fatigue crack initiation. In this study, the severe microstructural heterogeneity resulting from the significant difference of grains leads to the occurrence of large stress concentration at the boundary between the SZ and TMAZ. Moreover, the large grains in the TMAZ at the joint surface reduce the resistance of crack initiation, which makes the fatigue crack initiate at the grain boundary more easily. Above all, the fatigue fracture mainly occurs at the boundary between the SZ and TMAZ (Fig. 6a), and the large grain in TMAZ becomes the root of the shell pattern after fracturing. The SZ top surface possesses finer grains compared with the SZ bottom surface, which results in a severer change of grain size from TMAZ to SZ at the joint top surface. Therefore, the stress concentration at the joint top surface is higher than that at the joint bottom surface, and the fatigue crack is prone to initiate at the top part of boundary between SZ and TMAZ.

It can be found that the shell pattern is also formed in Fig. 7e and its area is smaller compared with the shell pattern in Fig. 7a. During the crack propagation process, the connected region of

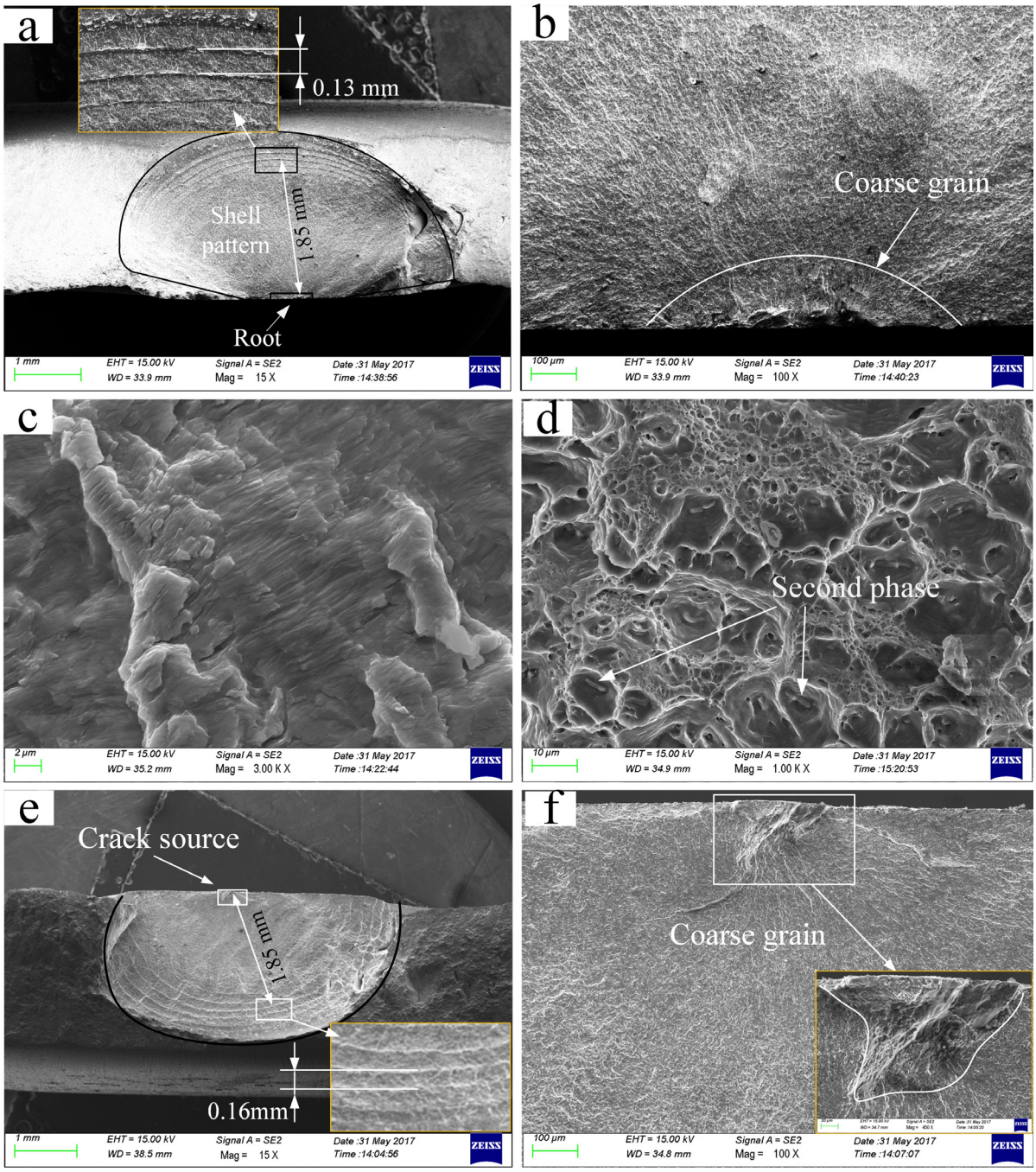

Fig. 7. Fracture morphologies: (a) specimen with stress level of 56% and its region of (b) fatigue source, (c) crack propagation, (d) final fast fracture; (e) specimen with stress level of 62% and its (f) fatigue source

the joint becomes smaller and smaller with the propagating of the fatigue crack, and then the final fracture occurs when the rest connected region cannot bear the maximum value of the cyclic stress. The smaller stress always leaves a smaller connected region before the final fracture. Therefore, the fatigue propagation region is bigger under the smaller stress level, resulting in a bigger shell pattern. The distance between the arcs (1.85 mm away from the crack source) is ~0.16 mm in this shell pattern, which is bigger than that of the specimen under the stress level of 56% (Fig. 7a). The appearance of arcs on the fracture surface indicates the change of the stress during the fatigue crack propagation process and the gap between two arcs is proportional to the stress level [35]. Generally, the bigger stress level always leads to a bigger gap.

The fracture surface of the specimen with a relatively low fatigue life (1081145) under the stress level of 56% is shown in Fig. 8. The morphology of the fracture surface located in the SZ is different from that located at the boundary between the SZ and TMAZ (Fig. 7a). A smooth and flat zone can be observed in the fracture surface (Fig. 8a). According to the report of Di et al. [8], this morphology may be related to the existence of zigzag curves in the SZ (Fig. 6b). A linear fatigue source is located in the middle of this zone and its enlarged view is displayed in Fig. 8b. The linear region is featured by a horizontal texture, and its adjacent

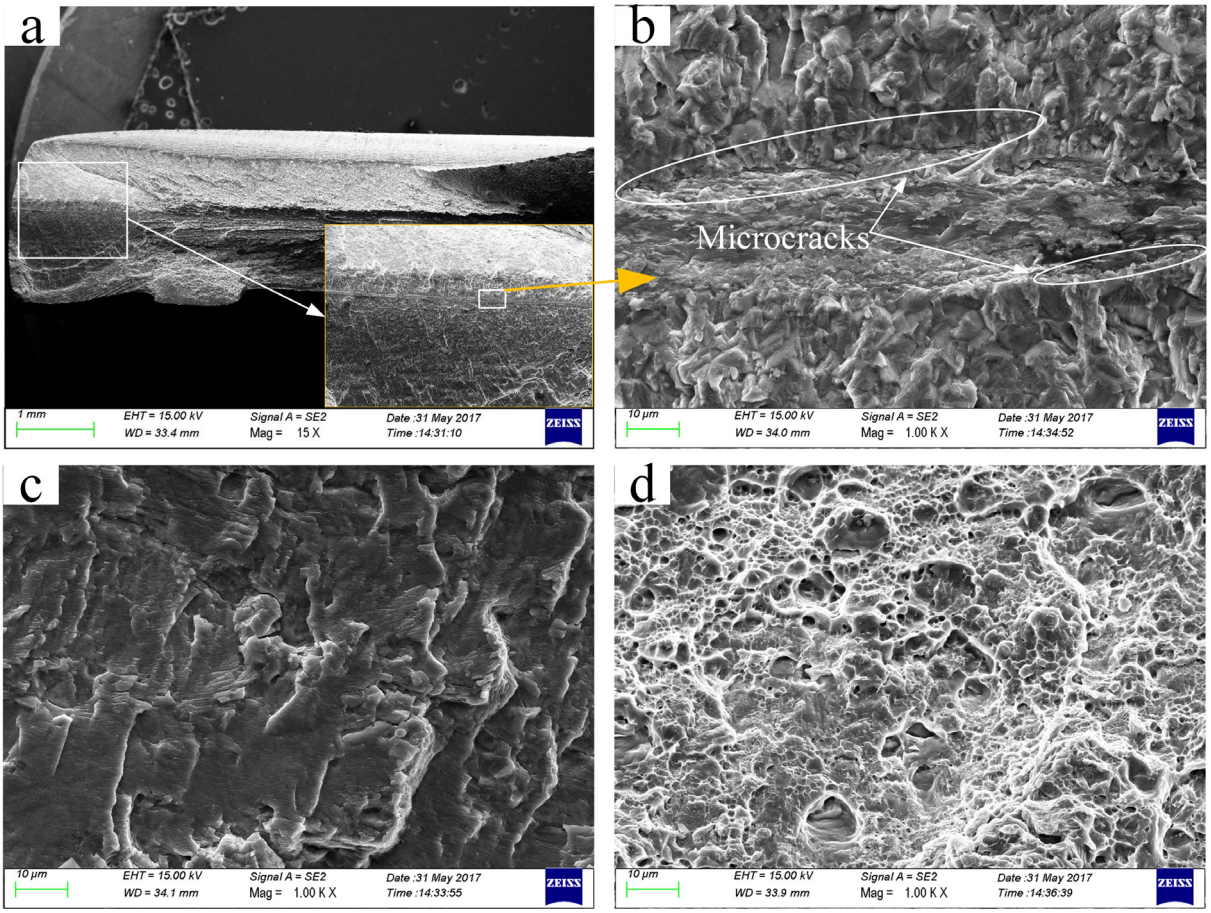

Fig. 8. Fracture morphologies of (a) specimen with low fatigue life under stress level 56% and its region of (b) fatigue source, (c) crack propagation, (d) final fast fracture

region is characterized by a rough vertical texture with the bare grains. Moreover, the microcracks are formed at the boundaries between those two regions (Fig. 8b). This texture difference results from the junctions caused by the plastic material flow with different directions in the SZ, which has been thoroughly discussed by Wu et al. [15]. The vicinity of the junction is the relatively weak bonding region with high stress concentration in the SZ, and the fatigue crack usually initiates in this region, resulting in the linear fatigue source.

The linear fatigue source facilitates the fatigue crack initiating at several locations, leading to the decrease of fatigue life. After initiation, the cracks rapidly coalesce and propagate along the zigzag curve, resulting in the flat and smooth region as mentioned above. Although fine-equiaxed grains can increase the resistance of cracks initiation in the SZ, they also bring an increased fatigue crack propagation (FCP) rate due to the high stored energy [25]. Therefore, the low fatigue life of the joint is attributed to the linear fatigue source and higher FCP rate in the SZ. As shown in Fig. 8c, the crack propagation region presents a quasi-cleavage morphology and there exist many tear ridges, second cracks and fragmentary planes. The fatigue striations intermittently spread over the planes and are difficult to be figured out. Fig. 8d presents the enlarged view of the final fracture region which is characterized by numerous dimples. However, the dimples in this fracture surface are smaller and shallower than those in the fracture surface with a high fatigue life (Fig. 7d). Therefore, compared with the specimen fracturing at the boundary between SZ and TMAZ (Fig. 7), the specimen fracturing in the SZ possesses a relatively low plasticity.

4. Conclusions

The hollow-extruded 6005A-T6 alloy profile was welded by FSW and then the welding joints milled from the profile were obtained. The uniaxial tension fatigue performance of the FSW joint was mainly investigated under high cycle and the following conclusions can be drawn.

(1) The BM possesses a layered microstructure and its grains with quite different morphologies along the thickness direction are all transformed into fine-equiaxed grains in the SZ after welding.

(2) The large recrystallization grain of the outer layer in the TMAZ is the main fatigue source due to the high stress concentration resulting from the large variation gradient of grain size between SZ and TMAZ. Therefore, most of fatigue specimens fracture at the boundary between the SZ and TMAZ rather than the region with the lowest microhardness. However, the specimen fracturing in the SZ possesses a low fatigue life.

(3) Due to the microstructural heterogeneity of the joint, the shell pattern, as the typical morphology, exists in the fracture surface located at the boundary between SZ and TMAZ. The gap between the arcs near the edge of the shell pattern is increased with the increase of stress level.

(4) The *S*-*N* curve is obtained under the stress ratio of 0.06, and the fatigue limit of the joint reaches 128.1 MPa which is 55% of joint tensile strength.

REFERENCES

[1] W.F. Xu, H.J. Liu, D.L. Chen, G.H. Luan, Int. J. Manuf. Technol. **74** (1-4), 209-218 (2014).

[2] K. Krasnowski, Arch. Metall. Mater. **59** (1), 157-162 (2014).

[3] C. Hamilton, S. Dymek, M. Blicharski, Arch. Metall. Mater. **53** (4), 1047-1054 (2008).

[4] N. Nanninga, C. White, Int. J. Fatigue **31**, 1215-1224 (2009).

[5] N. Nanninga, C. White, T. Furu, O. Anderson, R. Dickson, Int. J. Fatigue **30**, 1569-1578 (2008).

[6] N. Nanninga, C. White, R. Dickson, J. Mater. Eng. Perform. **20** (7), 1235-1241 (2010).

[7] P. Dong, D. Sun, H. Li, Mater. Sci. Eng. A **576**, 29-35 (2013).

[8] S.S. Di, X.Q. Yang, D.P. Fang, G.H. Luan, Mater. Chem. Phys. **104**, 244-248 (2007).

[9] C.Y. Deng, H. Wang, B.M. Gong, X. Li, Z.Y. Lei, Int. J. Fatigue **83**, 100-108 (2015).

[10] Z.H. Zhang, W.Y. Li, J.L. Li, Y.J. Chao, Int. J. Adv. Manuf. Technol. **73**, 1213-1218 (2014).

[11] S.D. Ji, Z.W. Li, Z.L. Zhou, L.G. Zhang, J. Mater. Sci. Technol. **90** (9), 3045-3053 (2017).

[12] P. Lacki, W. Więckowski, P. Wieczorek, Arch. Metall. Mater. **60** (3), 2297-2306 (2015).

[13] B. Rams, A. Pietras, K. Mroczka, Arch. Metall. Mater. **59** (1), 385-392 (2014).

[14] H.J. Liu, H. Fuji, M. Maeda, K. Nogi, J. Mater. Process. Technol. **142**, 692-696 (2003).

[15] M. Wu, C.S. Wu, S. Gao, J. Manuf. Process. **29**, 85-95 (2017).

[16] K. Krasnowski, Arch. Metall. Mater. **59** (1), 157-162 (2014).

[17] H. Aydin, M. Tutar, A. Durmus, A. Bayram, T. Sayaca, Trans. Indian. Inst. Met. **65** (1), 21-30 (2012).

[18] X.M. Zhang, D. Feng, X.K. Shi, S.D. Liu, Trans. Nonferrous. Met. Soc. China. **23**, 765-772 (2013).

[19] S.D. Ji, X.C. Meng, J.G. Liu, L.G. Zhang, S.S. Gao, Mater. Des. **62**, 113-117 (2014).

[20] H.J. Liu, X.Q. Liu, X.G. Wang, T.H. Wang, S. Yang, Int. J. Adv. Manuf. Technol. **88**, 1-11 (2016).

[21] Z.L. Liu, Y. Wang, S.D. Ji, Z.W. Li, Mater. Sci. Technol. **34** (2), 1-11 (2017).

[22] Y.C. Chen, H.J. Liu, J.C. Feng, Mater. Sci. Eng. A **420**, 21-25 (2006).

[23] Z.H. Zhang, W.Y. Li, Y. Feng, J.L. Li, Y.J. Chao, Acta. Mater. **92**, 117-125 (2015).

[24] Y. Yue, Z. Li, S. Ji, Y. Huang, Z. Zhou, J. Mater. Sci. Tech. **32**, 671-675 (2016).

[25] Q.L. Dai, Z.F. Liang, G.Q. Chen, L.C. Meng, Q.Y. Shi, Mater. Sci. Eng. A **580**, 184-190 (2013).

[26] T.H. Tra, M. Okazaki, K. Suzuki, Int. J. Fatigue **43**, 23-29 (2012).

[27] Y. Huang, X. Meng, Y. Zhang, J. Cao, J. Feng, J. Mater. Process. Tech. **250**, 313-319 (2017).

[28] Y. Huang, Y. Xie, X. Meng, Z. Lv, J. Cao, J. Mater. Process. Tech. **252**, 233-241 (2018).

[29] S.D. Ji, Y.Y. Jin, Y.M. Yue, S.S. Gao, Y. X. Huang, L. Wang, J. Mater. Sci. Technol. **29**, 955-960 (2013).

[30] P. Dong, H. M. Li, D.Q. Su n, W.B. Gong, J. Liu, Mater. Des. **45**, 524-531(2013).

[31] W. Sylwestrowicz, E. Hall, The deformation and ageing of mild steel III discussion of results. Proc. Phys. Soc. Sect. B. **64** (9), 495-502 (1951).

[32] C.Z. Zhou, X.Q. Yang, G.H. Luan, Scripta. Mater. **53**, 1187-119 (2005).

[33] M. Ericsson, R. Sandström, Int. J. Fatigue **32**, 302-309 (2010).

[34] C. He, Y.J. Liu, J.F. Dong, Q.Y. Wang, D. Wagner, C. Bathias, Int. J. Fatigue **82,** 379-386 (2016).

[35] J. Hoshino, Bull. JSME. **4** (13), 33-40 (2008).